Version of Record: https://www.sciencedirect.com/science/article/pii/S0378517320302283
Manuscript_5ccd1f1099ef85ed0a460c083543b965

Design of surface ligands for blood compatible gold nanoparticles: effect of charge and binding energy

Jordan Beurton[1,2], Philippe Lavalle[2], Arnaud Pallotta[1], Thomas Chaigneau[1], Igor Clarot[1], Ariane Boudier[1]*

Adresses

[1]: Université de Lorraine, CITHEFOR, Nancy, France

[2]: Université de Strasbourg, Faculty of Medicine, Inserm UMR 1121 Biomaterials and Bioengineering, Strasbourg, France

*Corresponding author: ariane.boudier@univ-lorraine.fr

© 2020 published by Elsevier. This manuscript is made available under the CC BY NC user license
https://creativecommons.org/licenses/by-nc/4.0/

Abstract

Gold nanoparticle (AuNP) interaction with the blood compartment as a function of their charge and the binding energy of their surface ligand was explored. Citrate, polyallylamine and cysteamine stabilized AuNP along with dihydrolipoic acid and polyethylene glycol capped AuNP were synthesized and fully characterized. Their interactions with model proteins (human albumin and human fibrinogen) were studied. Complexes formed between AuNP and protein revealed several behaviors ranging from corona formation to aggregation. Protein fluorescence quenching as a function of temperature and AuNP concentration allowed the determination of the thermodynamic parameters describing these interactions. The hemolysis induced by AuNP was also probed: an increasing or a decreasing of hemolysis ratio induced by AuNP was observed as of function of protein corona formation. Taken together, our results drew up a composite sketch of an ideal surface ligand for blood compatible AuNP. This capping agent should be strongly bound to the gold core by one or more thiol groups and it must confer a negative charge to the particles.

Keywords: Inorganic Nanoparticles, Surface Chemistry, Protein Adsorption, Thermodynamic Parameters, Hemolysis

1. Introduction

Gold nanoparticles (AuNP) are part of the most developed and used nanomaterials because of their ease of synthesis and their characteristics. They are well defined by their physicochemical and optical properties. AuNP can be functionalized by biomolecules and drugs with important yields due to a huge surface over volume ratio (Daniel & Astruc, 2004). The abundance of possible ligands creates a wide variety of objects, in terms of surface charge (zeta potential) or hydrodynamic diameter. The newly synthesized particles are surrounded by a more or less displaceable shell depending on the ligand binding energy. Among their various uses, these particles can be used as biosensors, drug delivery systems or contrast agents (Mieszawska et al., 2013) involving their intravenous injection. The bloodstream is a highly complex medium in which AuNP can interact with a wide variety of proteins or cells. According to the Vroman's effect (Vroman, 1962), the interaction between AuNP and plasma proteins is a dynamic system. During this sequential adsorption, a heterogeneous corona is formed with proteins with an increasing affinity for the AuNP. This phenomenon determines the biological identity of the particles and manages not only their bioavailability and pharmacokinetics but also their possible toxicity (Wang et al., 2015). Several studies already probed the interaction of proteins with AuNP as a function of their size, shape, charge... As examples, the variation of the nanoparticle hydrodynamic diameter revealed an influence on their internalization in cells trough endocytosis or micropinocytosis or in hemolysis induction (Purohit et al., 2016). Lacerda *et al.*, reported an increasing affinity between fibrinogen and citrate capped AuNP as a function of their hydrodynamic diameters (Lacerda et al., 2010). A shape dependence in the protein activation and cellular uptake was also described. Xie *et al.*, observed an increased internalization linked to AuNP shape (from stars and rods to triangles, respectively) (Xie et al., 2017). Quach and Kah demonstrated that

gold nano-spheres, -stars and -rods bearing polyethylene glycol (PEG) groups were able to induce complement activation (Quach and Kah, 2017). Through all these studies, all types of interactions between NP and proteins have been reported, from the weakest (Van der Walls and/or hydrogen bonds) to the strongest (covalent bound) (Shemetov et al., 2012). Thus, ligand exchange phenomena (NP surface ligand *vs* blood protein), especially with low-energy surface stabilizers, are of particular importance for the protein corona formation. However, the influence of functional groups binding the NP gold core in terms of binding energy is rather poorly reported. Thus, our work aimed at filling the information gap on the influence of the ligand characteristics on AuNP blood compatibility. We hypothesized that this is a key factor that governs the stability of the particles as soon as they are injected into the bloodstream. Besides, the ability of the ligand, to be more or less displaced, induces a selection of the proteins forming the corona. Therefore, the binding energy of the ligand influences the plasmatic mean residence time of the particles and therefore their biodistribution and pharmacokinetics.

In this work, we considered that the prediction of AuNP blood compatibility is a multifactorial equation in which the variables are the ligand characteristics (binding energy and charged groups) and the protein characteristics. We synthesized five different types of AuNP with characteristics and ligands frequently described in the biomedical field. Thus, AuNP-citrate, stabilized trough weak interactions with carboxylate groups, are often used as precursors for further functionalization steps through ligand exchange. AuNP stabilized by poly(allylamine) (PAH), a cationic polymer carrying primary amines able to bound the particle gold core were selected as models of positive nanoparticles with a weak ligand. AuNP stabilized by a cationic polymer can be used to create multilayered coated particles for a drug delivery purpose (Reum et al., 2010). We also selected AuNP capped by a ligand carrying one or more thiols. Positively charged particles were obtained with cysteamine. Here, the

interaction with the gold core was predominantly driven by the thiol group thanks to sulfur atom avidity for gold largely greater than the one between amine and gold. PEG capping allowed the synthesis of neutral particles and it is the gold standard for giving a protein antifouling ability to AuNP. Herein, a PEG bearing two thiol groups was chosen for better anchoring of the ligand on the gold core (Zopes et al., 2013). This also allowed the formation of looped PEG chains on the AuNP, which are known to have better biocompatibility, salt resilience and enhanced hydrophilicity (Du et al., 2019). AuNP were also synthesized using dihydrolipoic acid (DHLA), providing negatively charged particles with a strongly bound ligand (by two thiols per molecule). DHLA has the advantage of adding a carboxylic acid to AuNP surface allowing an easy functionalization through amide bond formation (Roux et al., 2005).

Based on the Vroman's effect, two different proteins were selected: albumin (firstly bound) and fibrinogen (latterly bound) as models (described in Table 1.) for probing AuNP-plasma proteins interaction. We investigated the physicochemical characterization of [AuNP, Protein] complexes as of function of particle charge and ligand binding energy using dynamic light scattering and spectrophotometry. The fluorescence quenching of albumin and fibrinogen at several temperatures and AuNP concentrations was measured. Thermodynamic parameters (Bi et al., 2004) of proteins interacting with anionic, cationic or neutral AuNP were determined. Lastly, the hemolysis induced by AuNP as a function of their characteristics was also probed. Our study showed that not only the particle charge but also the ligand binding energy determine the formation of the protein corona on NP. Those new objects display a different reactivity towards the blood compartment as observed in the hemolysis induction.

2. Materials & Methods

2.1 Reagents and standards

All reagents and solvents were of analytic grade and were used without further purification. Ultrapure deionized water (> 18.2 MΩ cm) was used for the preparation of all solutions. Polyallylamine hydrochloride (PAH) with average molecular masse of 17,500, cysteamine hydrochloride, dihydrolipoic acid (DHLA), sodium citrate, di-thiolated polyethylene glycol (PEG) with an average molecular mass of 8000, $HAuCl_4$, $NaBH_4$, human serum albumin and human fibrinogen were supplied by Sigma Aldrich. Wistar rat whole blood collected in heparin blood collection tubes was provided by our laboratory animal house. Na_2HPO_4, KH_2PO_4, KCl and NaCl were purchased from VWR Chemicals. Phosphate buffer saline solution (PBS) at 0.15 M was prepared as follows: $[Na_2HPO_4] = 6.68 \times 10^{-3}$ M, $[KH_2PO_4] = 1.47 \times 10^{-3}$ M, $[NaCl] = 138.00 \times 10^{-3}$ M, and $[KCl] = 2.68 \times 10^{-3}$ M, final pH was adjusted to 7.40. 50 nM Human albumin and human fibrinogen were prepared by diluting a 1 µM stock solution in PBS.

2.2 AuNP synthesis

Citrate stabilized AuNP were synthesized in aqueous solution according to our previous work (Tournebize et al., 2012). Under inert atmosphere, 1 mL of $HAuCl_4$ solution (10 mg/mL) was added into 90 mL of water and then 2 mL of sodium citrate 55 mM. The solution was stirred for 1 min then 1 mL of $NaBH_4$ 19 mM was added and the solution was stirred for 10 min. AuNP DHLA and PEG were obtained through ligand exchange with previously described AuNP. 10 mL of 60 mM DHLA or dithiolated PEG solutions prepared in NaOH 0.5 M were added to 25 mL of AuNP citrate. After an overnight reaction, AuNP were dialyzed twice against PBS for 24 h. AuNP-PAH were synthesized with the same method as AuNP citrate using 1 mL of 87 mM of PAH solution as stabilizing ligand. AuNP cysteamine were

synthesized by a two steps reduction method. At first, 90 mL of ultra-pure water added with 1 mL of $HAuCl_4$ solution (10 mg/mL) and 1 mL of cysteamine hydrochloride 27 mM. This solution was heated using a heating sand bath (250 °C) and a reflux system until it becomes colorless, corresponding to Au^{3+} reduction to Au^{+} by thiols. The second reduction Au^{+} to Au^{0} was performed by adding 50 µL of 19 mM of $NaBH_4$. Ionic gold quantification was performed on every synthesis with a previously developed in house method (Pallotta et al., 2018). Synthesis yields were found above 99.6 % for each kind of AuNP.

2.3 AuNP characterization

Colloidal gold nanoparticles were characterized after synthesis without any dilution step. UV–vis spectrophotometer (UV-1800 Shimadzu) was used for spectra recordings and absorbance measurements. The hydrodynamic diameter in volume mode (Dh) and zeta potential (ζ) of AuNP were measured at 20 ± 1 °C with a backscattering detection angle of 173°. Zeta potential was calculated after the conversion of electrophoretic mobility values measured by laser Doppler velocimetry using the Smoluchowski's equation. Both, DLS and laser Doppler velocimetry measurements were conducted on a Zeta Sizer nanoseries Nano-ZS fitted with a helium-neon laser performing at 633 nm (Malvern Instruments, UK). Transmission Electron Microscopy (TEM) images were recorded using a Philips CM20 instrument with a LaB6 cathode at 200 kV and with CF200-CU carbon covered copper grids. DigitalMicrograph software was used to determine AuNP cores diameters, Dc, by measuring at least 150 individualized nanoparticles.

2.4 Interaction of AuNP and proteins studied by spectrophotometry and dynamic light scattering

153 Concentrations of AuNP ranging from (3.5 nM to 21 nM for Citrate, PAH, Cysteamine
154 stabilized AuNP and DHLA, PEG capped AuNP), corresponding to a quantity of 10^{12} to 10^{13}
155 particles per samples were used. AuNP concentrations were comparable to those used in
156 biodistribution studies after intravenous injection. For example, (Zhang et al., 2009) and
157 (Semmler-Behnke et al., 2008) studied AuNP biodistribution in mice and rats after injection
158 of quantities ranging from 1×10^{12} to 9×10^{13} and 4×10^{12} to 4×10^{13} per animals
159 respectively. All AuNP dilutions were prepared in PBS 0.15 M pH = 7.4 containing albumin
160 or fibrinogen with a final concentration of 50 nM. Visible spectra (400 – 800 nm) and
161 hydrodynamic diameters were acquired just after mixing at 20 ± 1 °C. Results are reported as
162 the main hydrodynamic diameters measured in volume. External layer thickness (sum of the
163 ligand layer, the protein corona and the solvation shell) was determined by subtracting the
164 AuNP Dc to the Dh of [AuNP, Protein] complexes.

165 2.5 Fluorescence quenching study and constants determinations.

166 The analysis of AuNP and proteins interaction was performed trough fluorescence quenching
167 experiments as a function of temperature (4 °C, 20 °C, 37°C and 50 °C) and AuNP
168 concentration (3.5 nM to 21 nM). Albumin and fibrinogen concentrations were kept constant
169 (50 nM). This concentration was chosen greater than AuNP concentration and with a
170 sufficient fluorescence signal for quenching studies. Proteins solutions, PBS and AuNP were
171 pre-incubated at 4 °C, 20 °C, 37°C or 50 °C before mixing and measurements. The
172 fluorescence intensity was measured immediately after sample preparation using a quartz
173 cuvette with a light path 10x4 mm (Hellma Analytics, Müllheim, Germany). Hitachi F-2000
174 Fluorescence Spectrophotometer equipped with a Xenon lamp and with a temperature-
175 controlled analysis chamber was used to perform the assay. The excitation and emission

wavelengths were set at 280 ± 5 nm and 340 ± 5 nm, respectively. Sensitivity was set in high mode for albumin conditions and on medium for fibrinogen.

The protein fluorescence quenching relied on the interaction of albumin or fibrinogen with AuNP assimilated to a ligand according to the following equation (1):

$$\mathrm{AuNP} + \mathrm{Protein} \overset{\mathrm{Ka}}{\rightarrow} [\mathrm{AuNP},\ \mathrm{Protein}] \quad (1)$$

Ka being the affinity constant. For referring to the formation of this complex, in the text the following notation was used [AuNP-X/@X, albumin or fibrinogen], where -X or @X represent the stabilizing or capping ligand under consideration, respectively.

The fluorescence quenching mechanism was determined with the Stern-Volmer equation (2):

$$\frac{F_0}{F} = 1 + K_q \tau_0 [AuNP] = 1 + K_{SV}[AuNP] \quad (2)$$

In which, F_0 and F are the fluorescence intensities of albumin or fibrinogen in the absence and presence of quencher (AuNP), respectively. K_{SV} is the Stern-Volmer quenching constant, K_q the quenching constant, [AuNP] the molar concentration of AuNP and τ_0 is the lifetime of albumin and fibrinogen without quencher, which was considered as 10^{-7} s.

Static quenching allows the calculation of affinity constant (Ka) and Hill coefficient (n) with the following equation (3):

$$\log \frac{F_0 - F}{F} = \log Ka + n \log[AuNP] (3)$$

Previously mentioned constants were determined by plotting $\log \frac{F_0 - F}{F}$ versus $\log [AuNP]$. Slopes and intercepts of the resulting curves represented Hill coefficient and $\log Ka$ respectively.

Entropy (ΔS) and enthalpy (ΔH) variations were determined with the Van't Hoff model. Previously mentioned constants were determined by plotting $\ln Ka$ as a function of $\frac{1}{T}$, where T is the temperature in K.

Slopes and intercepts of the resulting curves respectively represented $\frac{-\Delta H}{R}$ and $\frac{\Delta S}{R}$.

R being the perfect gas constant taken equal to 8.314 $J.K^{-1}.mol^{-1}$.

Gibbs free energy (ΔG) was calculated with the following equation (4):

$$\Delta G = -RT \ln Ka \quad (4)$$

2.6 AuNP induced hemolysis

AuNP ability to induce hemolysis was adapted from a previously described method (Pallotta et al., 2017) using blood from a Wistar male rat. Briefly, Red Blood Cells (RBC) washing was performed after centrifugation (20 min, 3000 rpm, 4 °C) by substituting the plasma by the same volume of NaCl 0.9 % (m/v). A stock solution was prepared by mixing 1 mL of previously described RBC solution and 1.25 mL of NaCl 0.9 % (W/V). Working solutions were obtained by a 25-fold dilution on PBS alone, with albumin or fibrinogen. Positive and negative controls were obtained through the same dilutions in ultra-pure water or PBS, respectively. Protein (albumin and fibrinogen) final concentration was 50 nM and AuNP concentration ranged from 3.5 to 21 nM. PBS was preferred instead of NaCl 0.9 % to ensure the same proteins protonation state as *in vivo*. Samples were prepared in triplicates and incubated in a shaking and heating water bath (80 oscillations.min^{-1} and 37 °C) during 2 h. The hemolysis rate was determined by measuring the absorbance of the samples at λ = 541 nm after centrifugation (10 min, 5 000 rpm). Hemolysis rates induced by AuNP were expressed as a percentage of the hemolysis found with the positive control.

224 3. Results and Discussion

225 3.1 Nanoparticles characterization

226 Several types of gold nanoparticles were synthesized using stabilization agent of various
227 chemical nature with increasing binding energy for Au core: carboxylate groups for citrate
228 ions, amine groups for PAH, thiol groups for cysteamine and dithiol groups for DHLA and
229 PEG. Their physicochemical characterization was performed, and the results are presented in
230 Table 2. and Figure 1. Spectrophotometric properties of these particles showed a single
231 plasmon band (λ_{max}) characteristic of metallic nanoparticles. No other peak was detected,
232 meaning that little to none aggregation was observed. This was confirmed by transmission
233 electron microscopy observations that showed spherical and individualized particles.
234 Hydrodynamic diameters (Dh) and core diameters (Dc) measurement allowed the
235 determination of AuNP stabilization and solvation layers thickness. The use of different
236 ligands during synthesis provided negatively charged NP (AuNP-Citrate and @DHLA), or
237 neutral particles (AuNP@PEG) or positively charged NP (AuNP-PAH and @Cysteamine)

238 3.2 Protein effect on AuNP physicochemical characterization

239 Albumin and fibrinogen were selected as models for studying the interaction of AuNP with
240 blood proteins. Albumin is known to be a ubiquitous carrier able to rapidly bound on NP. In a
241 second step, this non-specific binding is replaced by complexation with other more
242 specialized blood proteins such as fibrinogen corresponding to the Vroman's effect. The study
243 of the physicochemical characterization of AuNPs in the presence of these two proteins
244 represents a first step towards understanding the fate of AuNP in blood.

245

246 3.2.1 Modification of AuNP optical properties

247 The interaction of [AuNP, Protein] and its effect on their optical properties were studied by
248 visible spectrophotometry (Figure 2.). Variation of the Surface Plasmon Band was studied by
249 mixing an increasing concentration of AuNP with a constant concentration (50 nM) of either
250 albumin or fibrinogen. This physicochemical parameter is specific to metallic nanoparticles
251 and gives information on their size, their form, their surrounding medium, and neighbors
252 particularly the inter-nanoparticular distance (Amendola et al., 2017). As reported in the
253 histograms a redshift of the plasmon band was observed, corresponding to NP surrounding
254 modification due to proteins. The highest increases in maximal wavelength were observed for
255 citrate, PAH and cysteamine AuNP (Figure 2. A, B, C) reflecting a significant impact on the
256 physicochemical properties of these particles after protein binding. Plasmon band broadening
257 was related to an increase of AuNP size dispersion (Moores and Goettmann, 2006) due to the
258 formation of a protein corona around them and/or to the formation of aggregates. For DHLA
259 and PEG AuNP (Figure 2. E, F) these changes were less pronounced representing a limited
260 impact of proteins on these particles.

261

3. 2.2 Variation of AuNP Dh induced by proteins

The variation of Dh as a function of AuNP concentration with either albumin or fibrinogen was probed (Figure 3.). Differences between AuNP Dc and Dh gave an estimation of the surrounding layer thickness. This external layer thickness was defined as the sum of the ligand layer, the protein corona and the solvation shell. It was calculated only when particles were not aggregated. Values of typical diameters measured or estimated at AuNP concentration of 7 nM are listed in Table 3. AuNP-citrate Dh were found more important in presence of albumin than without. Still, for this kind of AuNP, the Dh stayed stable at any NP concentration, suggesting the formation of a stable protein corona on individualized particles. At the opposite, as far as AuNP-citrate are concerned, the formation of increasingly important aggregates was observed in the presence of fibrinogen. For PAH stabilized nanoparticles large aggregates over 500 nm were observed in both protein conditions at any AuNP concentrations revealing an important instability of these particles in a biological-like medium. Hydrodynamic diameters of cysteamine nanoparticles increased gradually for both albumin and fibrinogen conditions, highlighting an aggregation mediated by AuNP concentration. Fibrinogen tendency to form large aggregates or to induce the formation of thicker corona compared to albumin is due to its shape and dimensions (Table 1.), in fact, this protein is able to bridge several nanoparticles or to be organized as a loop on a single particle (Deng et al., 2012). Hydrodynamic diameters of DHLA and PEG particles were found to be stable over the whole range of the studied AuNP concentration.

3.3. Mechanism of AuNP binding to protein

As reported in Table 1, albumin and fibrinogen both carry tryptophan residues which fluorescence can be quenched as a function of the presence of various compounds. Then, a thorough characterization of AuNP-protein interactions was allowed through fluorescence

study. Thermodynamics parameters, quenching, K_{SV}, and affinity, Ka, constants were determined for both proteins and as a function of AuNP surface ligands.

3.3.1. Quenching constants

Fluorescence quenching studies relied on the native fluorescence (F_0) of proteins mainly carried by tryptophan residues. The addition of molecules or particles able to bind on protein induces a fluorescence quenching. Then, a decreasing fluorescence intensity (F) was observed when AuNP concentration was increased. Plotting of F_0/F as a function of AuNP concentrations (Figure 4.) allowed the determination of Stern-Volmer constant (K_{SV}) for albumin and fibrinogen. In all the studied conditions, the quenching rate constant (Kq) was greater than the maximum diffusion collision quenching rate constant (2×10^{10} $L.mol^{-1}.s^{-1}$ (Bi et al., 2004)) meaning that the fluorescence quenching relied on the formation of a static complexes ([AuNP, Albumin] and [AuNP, Fibrinogen]). For a static quenching, the interaction site between AuNP and protein is located in the close vicinity (between 10 Å and 100 Å (Swathi and Sebastian, 2009)) of the fluorophores (tryptophan) and the distance between protein and quencher stays constant, on the contrary to a collisional or dynamic complex.

3.3.2 Thermodynamics constants of AuNP proteins interaction

Plotting of $\log\frac{F_0-F}{F}$ as a function of $\log[AuNP]$ values at 37 °C (Figure 5.) gave the parameters listed in Table 5. Hill coefficient can also be defined as a measure of binding cooperativity. The value lower than 1 obtained for [AuNP@DHLA, Albumin] corresponds to an anticooperative binding indicating that the association energy per particle progressively decreases with further protein adsorption. For AuNP citrate, PAH, cysteamine, Hill

coefficient was found greater than 1 meaning that their interaction with either albumin or fibrinogen relied on a cooperative binding. The association energy increases gradually as long as particles bind on proteins. In the case of [AuNP@DHLA, Fibrinogen] and [AuNP@PEG, Fibrinogen], Hill coefficient was equal to 1 indicating that the association energy of these complexes was not varying as a function of protein adsorption. Besides, ΔG negative values revealed a spontaneous formation of all the [AuNP, Protein] complexes. Affinity constant (Ka) was found greater than 10^3 (excepted for [AuNP@DHLA, Albumin]), indicating a high affinity between each type of AuNP and either albumin or fibrinogen. In the case of the [AuNP@DHLA, Albumin], a low Ka value was found, suggesting a moderate affinity for the complex formation.

Entropy and enthalpy variations signs and values (ΔS and ΔH, respectively) allowed the determination of the types of chemical interactions between AuNP and proteins.The negative ΔS and ΔH values obtained for [AuNP-citrate, Albumin], [AuNP-PAH, Albumin], [AuNP@cysteamine, Albumine], [AuNP@DHLA, Albumin] and [AuNP-PAH, Fibrinogen] are characteristics of an interaction based on Van der Waals and/or H-bond formation. These weak energy interactions are frequently managing contacts between particles and biomolecules. They allow stabilizing interactions between the solvating layers of each object as well as between their respective surfaces. The positive values of ΔS and ΔH are linked to hydrophobic interactions. A positive ΔS and a positive or negative value for ΔH indicate an ionic interaction. In this context, definitions of these two forces are important to understand the precise nature of the interactions leading to the complex formation. Hydrophobic association (Ross and Subramanian, 1981) is exclusively referring to the partial withdrawal of a nonpolar group from water and/or from the solvation layers of AuNP or proteins and not to an interaction between nonpolar groups themselves. The ionic association represents a neutralization of opposite charges (Manning, 1978). Here, the scale at which this interaction

334 occurs is an important consideration. This must be understood as an electrostatic interaction
335 between the particle and the protein and not between two net charges present on the different
336 objects. Considering those definitions, hydrophobic and ionic interactions found for
337 [AuNP@PEG, Albumin], [AuNP-citrate, Fibrinogen] and [AuNP@cysteamine, Fibrinogen]
338 relied on the modification of the species (non-polar and charged groups or ions) involved in
339 the solvation layers of AuNP and the protein resulting from the association. The ionic
340 association found for [AuNP@DHLA, Fibrinogen] is based on the interaction of negatively
341 charged AuNP@DHLA (carboxylate groups) and positively charged residues of fibrinogen.
342 Concerning [AuNP@PEG, Fibrinogen] an analogous phenomenon explains the ionic
343 interaction found. it has already been described that a PEG capping layer does not offer a total
344 screening of charge(Wang et al., 2013) carried by the particle gold core. In the case of
345 AuNP@PEG, the electron cloud of the core may stay mobilizable for electrostatic
346 interactions.

347 3.4 AuNP interaction with blood

348 AuNP were incubated with RBC without (Figure 6. A) or with albumin (Figure 6. B) and
349 fibrinogen (Figure 6. C) to probe their ability to induce hemolysis. For each condition and all
350 AuNP types, hemolysis was found increasing as a function of AuNP concentration.

351 In the first condition without protein (Figure 6. A), two opposite behaviors were identified.
352 Citrate and PAH stabilized and cysteamine capped AuNP induced a significant level of
353 hemolysis greater than 10 % from the lowest concentration. The mechanisms explaining these
354 results are based on AuNP surface ligands. It is commonly known that citrate ions with the
355 lowest binding energy for NP gold core (Table 2) are forming an easily displaceable shell.
356 These particles strongly interacted with RBC through ligand exchange with their membrane
357 components such as sialic acid. On the other side, cysteamine, a strongly bound ligand, could

not be removed. These positively charged NP interacted with negatively charged RBC membranes through electrostatic interactions. PAH, an intermediate strength ligand between carboxylic acid and thiol reacted through a combination of ligand exchange and charge interaction. Whereas for DHLA and PEG capped AuNP, hemolysis greater than 10 % was generated only at the highest concentration. Here, those particles are capped by non-displaceable ligands carrying two thiols. The low hemolysis rate found also relied on the negative charge of AuNP@DHLA and the steric hindrance provided by AuNP@PEG. Here, AuNP induced hemolysis was driven by two factors, ligand binding energy and the particle charge.

Addition of either albumin (figure 6. B) or fibrinogen (Figure 6. C) during the assay revealed a protein influence on the AuNP induced hemolysis. Considering the previous results showing the spontaneous formation of the static complex [AuNP, Protein], hemolysis should now be considered as being generated by new objects resulting from this association. The two previously described behaviors were still found. Concerning citrate and PAH stabilized AuNP and cysteamine capped AuNP at a concentration greater than 7 nM, hemolysis was found increased in presence of the proteins. The positive binding cooperativity (Hill coefficient, n >1) certainly promoted the interaction between the [AuNP, Protein] complexes and RBC. Furthermore, for those particles, the hemolysis ratio was more important with fibrinogen. This could be explained by the strongest affinity constants (Ka) and higher positive binding cooperativities found for fibrinogen compared to albumin, leading to the formation of larger aggregates.

On the other hand, hemolysis generated by [AUNP@DHLA, Albumin], [AUNP@DHLA, Fibrinogen], [AUNP@PEG, Albumin] and [AUNP@PEG, Fibrinogen] complexes was lower than the one induced by the 3 others particles. The values were not significantly different

382 from the negative control at low AuNP concentration. Even if the formation of static
383 complexes between those particles and proteins has been identified, spectrophotometric and
384 dynamic light scattering studies demonstrated a limited modification of AuNP
385 physicochemical parameters induced by proteins. Fluorescence quenching gave Hill
386 coefficient values less than or equal to one, suggesting that protein corona surrounding
387 AuNP@DHLA and AuNP@PEG did not promote the interaction of [AUNP@DHLA,
388 Albumin], [AUNP@DHLA, Fibrinogen], [AUNP@PEG, Albumin] and [AUNP@PEG,
389 Fibrinogen] complexes with RBC.

390 Taken altogether, these results fully described [AuNP, Protein] complexes interaction. Indeed,
391 the influence of proteins on nanoparticle characterization was probed through
392 spectrophotometric and dynamic light scattering studies. An important modification of citrate
393 and PAH stabilized and cysteamine capped AuNP physicochemical parameters was observed
394 in the presence of proteins. Weakly stabilized citrate AuNP remained in the nanoparticle form
395 with albumin but were aggregated with fibrinogen, showing that the protein nature is also an
396 important parameter (Zhang et al., 2014). Also, this study points out that working on solely
397 albumin represents a limited model for the study of protein - nanoparticle interaction.
398 Positively charged AuNP (PAH and cysteamine) formed aggregates with either albumin or
399 fibrinogen. Other studies have already shown such results. For example, it has been
400 demonstrated that cetyltrimethylammonium bromide (CTAB) stabilized AuNP aggregate with
401 albumin through electrostatic interactions (Boulos et al., 2013; Wang et al., 2019). Besides,
402 we showed here, that this aggregation also depends on the binding energy of the AuNP
403 surface ligands. Impact of the nanoparticles on the native fluorescence of proteins allowed
404 quenching studies and the determination thermodynamics constants describing those
405 interactions. It has been shown that the corona protein formation on AuNP is a dynamic
406 phenomenon responding to the Vroman's effect. At first, AuNP interact with unspecialized

protein such as albumin and then, they tend to be bound by other more specialized proteins. In this study, a higher affinity was found between all particles and fibrinogen rather than albumin. We also demonstrated that this affinity depends on the nature of the AuNP surface ligand. Lastly, many studies described the formation of protein corona on AuNP as a function of protein nature, of NP hydrodynamic diameter (Xiao et al., 2018) or medium conditions such as pH (Sotnikov et al., 2019). The conditions of corona formation, its evolution over time or its impact on the bioavailability of nanoparticles were previously published. In this work, we proved that hemolysis can be strengthened by the formation of this protein corona and to the best of our knowledge this article is the first to report this behavior.

Conclusion

Pulled together, our results drew up of the composite sketch of an ideal surface ligand for blood compatibles AuNP. The best capping agent should be strongly bound to the gold core by one or more thiols group and it must confer a negative charge to the particles.

Further studies are still required to fully describe the influence of AuNP surface ligand in the interaction with the blood compartment. Our future works will focus on AuNP effect on the coagulation and the inflammatory response. Indeed, thrombin activation as a function of AuNP nature or with the proteins of the complement pathway will be studied.

425 Acknowledgments

426 Authors thank laboratory animal house (ACBS) for providing rat whole blood. The authors
427 also acknowledge “Region Grand Est” for financial support.

428 Declarations of interest: none

429

430 References

431 Al-Johani, H., Abou-Hamad, E., Jedidi, A., Widdifield, C.M., Viger-Gravel, J., Sangaru, S.S.,
432 Gajan, D., Anjum, D.H., Ould-Chikh, S., Hedhili, M.N., Gurinov, A., Kelly, M.J., El
433 Eter, M., Cavallo, L., Emsley, L., Basset, J.-M., 2017. The structure and binding mode
434 of citrate in the stabilization of gold nanoparticles. Nat. Chem. 9, 890–895.
435 https://doi.org/10.1038/nchem.2752
436 Amendola, V., Pilot, R., Frasconi, M., Maragò, O.M., Iatì, M.A., 2017. Surface plasmon
437 resonance in gold nanoparticles: a review. J. Phys. Condens. Matter 29, 203002.
438 https://doi.org/10.1088/1361-648X/aa60f3
439 Bi, S., Ding, L., Tian, Y., Song, D., Zhou, X., Liu, X., Zhang, H., 2004. Investigation of the
440 interaction between flavonoids and human serum albumin. J. Mol. Struct. 703, 37–45.
441 https://doi.org/10.1016/j.molstruc.2004.05.026
442 Boulos, S.P., Davis, T.A., Yang, J.A., Lohse, S.E., Alkilany, A.M., Holland, L.A., Murphy,
443 C.J., 2013. Nanoparticle–Protein Interactions: A Thermodynamic and Kinetic Study of
444 the Adsorption of Bovine Serum Albumin to Gold Nanoparticle Surfaces. Langmuir
445 29, 14984–14996. https://doi.org/10.1021/la402920f
446 Cieśla, M., Adamczyk, Z., Barbasz, J., Wasilewska, M., 2013. Mechanisms of Fibrinogen
447 Adsorption at Solid Substrates at Lower pH. Langmuir 29, 7005–7016.
448 https://doi.org/10.1021/la4012789
449 Daniel, M. C., & Astruc, D. (2004). Gold nanoparticles: Assembly, supramolecular chemistry,
450 quantum-size-related properties, and applications toward biology, catalysis, and
451 nanotechnology. Chemical Reviews, 104(1), 293–346.
452 https://doi.org/10.1021/cr030698+

453 Deng, Z.J., Liang, M., Toth, I., Monteiro, M.J., Minchin, R.F., 2012. Molecular Interaction of
454 Poly(acrylic acid) Gold Nanoparticles with Human Fibrinogen. ACS Nano 6, 8962–
455 8969. https://doi.org/10.1021/nn3029953
456 Du, Y., Jin, J., Liang, H., Jiang, W., 2019. Structural and Physicochemical Properties and
457 Biocompatibility of Linear and Looped Polymer-Capped Gold Nanoparticles.
458 Langmuir acs.langmuir.9b00045. https://doi.org/10.1021/acs.langmuir.9b00045
459 Erickson, H.P., 2009. Size and Shape of Protein Molecules at the Nanometer Level
460 Determined by Sedimentation, Gel Filtration, and Electron Microscopy. Biol. Proced.
461 Online 11, 32–51. https://doi.org/10.1007/s12575-009-9008-x
462 Gonçalves, S., Santos, N.C., Martins-Silva, J., Saldanha, C., 2007. Fluorescence spectroscopy
463 evaluation of fibrinogen–β-estradiol binding. J. Photochem. Photobiol. B 86, 170–176.
464 https://doi.org/10.1016/j.jphotobiol.2006.09.001
465 Lacerda, S.H.D.P., Park, J.J., Meuse, C., Pristinski, D., Becker, M.L., Karim, A., Douglas,
466 J.F., 2010. Interaction of Gold Nanoparticles with Common Human Blood Proteins.
467 ACS Nano 4, 365–379. https://doi.org/10.1021/nn9011187
468 Manning, G.S., 1978. The molecular theory of polyelectrolyte solutions with applications to
469 the electrostatic properties of polynucleotides. Q. Rev. Biophys. 11, 179–246.
470 https://doi.org/10.1017/S0033583500002031
471 Mieszawska, A.J., Mulder, W.J.M., Fayad, Z.A., Cormode, D.P., 2013. Multifunctional Gold
472 Nanoparticles for Diagnosis and Therapy of Disease. Mol. Pharm. 10, 831–847.
473 https://doi.org/10.1021/mp3005885
474 Moores, A., Goettmann, F., 2006. The plasmon band in noble metal nanoparticles: an
475 introduction to theory and applications. New J. Chem. 30, 1121.
476 https://doi.org/10.1039/b604038c

Nuzzo, R.G., Zegarski, B.R., Dubois, L.H., 1987. Fundamental Studies of the Chemisorption of Organosulfur Compounds on Au(111). Implications for Molecular Self-Assembly on Gold Surfaces. J. Am. Chem. Soc. 109, 733–740.

Pallotta, A., Parent, M., Clarot, I., Luo, M., Borr, V., Dan, P., Decot, V., Menu, P., Safar, R., Joubert, O., Leroy, P., Boudier, A., 2017. Blood Compatibility of Multilayered Polyelectrolyte Films Containing Immobilized Gold Nanoparticles. Part. Part. Syst. Charact. 34, 1600184. https://doi.org/10.1002/ppsc.201600184

Pallotta, A., Philippe, V., Boudier, A., Leroy, P., Clarot, I., 2018. Highly sensitive and simple liquid chromatography assay with ion-pairing extraction and visible detection for quantification of gold from nanoparticles. Talanta 179, 307–311. https://doi.org/10.1016/j.talanta.2017.11.016

Purohit, R., Vallabani, N.S., Shukla, R.K., Kumar, A., Singh, S., 2016. Effect of gold nanoparticle size and surface coating on human red blood cells. Bioinspired Biomim. Nanobiomaterials 5, 121–131. https://doi.org/10.1680/jbibn.15.00018

Quach, Q.H., Kah, J.C.Y., 2017. Non-specific adsorption of complement proteins affects complement activation pathways of gold nanomaterials. Nanotoxicology 11, 382–394. https://doi.org/10.1080/17435390.2017.1306131

Reum, N., Fink-Straube, C., Klein, T., Hartmann, R.W., Lehr, C.-M., Schneider, M., 2010. Multilayer Coating of Gold Nanoparticles with Drug−Polymer Coadsorbates. Langmuir 26, 16901–16908. https://doi.org/10.1021/la103109b

Ross, P.D., Subramanian, S., 1981. Thermodynamics of protein association reactions: forces contributing to stability. Biochemistry 20, 3096–3102. https://doi.org/10.1021/bi00514a017

Roux, S., Garcia, B., Bridot, J.-L., Salomé, M., Marquette, C., Lemelle, L., Gillet, P., Blum, L., Perriat, P., Tillement, O., 2005. Synthesis, Characterization of Dihydrolipoic Acid

Capped Gold Nanoparticles, and Functionalization by the Electroluminescent Luminol. Langmuir 21, 2526–2536. https://doi.org/10.1021/la048082i

Semmler-Behnke, M., Kreyling, WG., Lipka, J., Fertsch, S., Wenk, A., Takenaka, S., Schmid, G., Brandau, W., 2008. Biodistribution of 1.4- and 18-nm gold particles in rats. Small, 4, 2108–2111. https://doi.org/10.1002/smll.200800922

Shemetov, A.A., Nabiev, I., Sukhanova, A., 2012. Molecular Interaction of Proteins and Peptides with Nanoparticles. ACS Nano 6, 4585–4602. https://doi.org/10.1021/nn300415x

Sotnikov, D.V., Berlina, A.N., Ivanov, V.S., Zherdev, A.V., Dzantiev, B.B., 2019. Adsorption of proteins on gold nanoparticles: One or more layers? Colloids Surf. B Biointerfaces 173, 557–563. https://doi.org/10.1016/j.colsurfb.2018.10.025

Swathi, R.S., Sebastian, K.L., 2009. Distance dependence of fluorescence resonance energy transfer. J. Chem. Sci. 121, 777–787. https://doi.org/10.1007/s12039-009-0092-x

Tournebize, J., Boudier, A., Sapin-Minet, A., Maincent, P., Leroy, P., Schneider, R., 2012. Role of Gold Nanoparticles Capping Density on Stability and Surface Reactivity to Design Drug Delivery Platforms. ACS Appl. Mater. Interfaces 4, 5790–5799. https://doi.org/10.1021/am3012752

Vroman, L., 1962. Effect of absorbed proteins on the wettability of hydrophilic and hydrophobic solids. Nature 196, 476–477. https://doi.org/10.1038/196476a0

Wang, G., Yan, C., Gao, S., Liu, Y., 2019. Surface chemistry of gold nanoparticles determines interactions with bovine serum albumin. Mater. Sci. Eng. C 103, 109856. https://doi.org/10.1016/j.msec.2019.109856

Wang, P., Wang, X., Wang, L., Hou, X., Liu, W., Chen, C., 2015. Interaction of gold nanoparticles with proteins and cells. Sci. Technol. Adv. Mater. 16, 034610. https://doi.org/10.1088/1468-6996/16/3/034610

527 Wang, W., Wei, Q.-Q., Wang, J., Wang, B.-C., Zhang, S., Yuan, Z., 2013. Role of thiol-
528 containing polyethylene glycol (thiol-PEG) in the modification process of gold
529 nanoparticles (AuNPs): Stabilizer or coagulant? J. Colloid Interface Sci. 404, 223–
530 229. https://doi.org/10.1016/j.jcis.2013.04.020
531 Xiao, W., Xiong, J., Zhang, S., Xiong, Y., Zhang, H., Gao, H., 2018. Influence of ligands
532 property and particle size of gold nanoparticles on the protein adsorption and
533 corresponding targeting ability. Int. J. Pharm. 538, 105–111.
534 https://doi.org/10.1016/j.ijpharm.2018.01.011
535 Xie, X., Liao, J., Shao, X., Li, Q., Lin, Y., 2017. The Effect of shape on Cellular Uptake of
536 Gold Nanoparticles in the forms of Stars, Rods, and Triangles. Sci. Rep. 7, 3827.
537 https://doi.org/10.1038/s41598-017-04229-z
538 Zhang, G., Yang, Z., Lu, W., Zhang, R., Huang, Q., Tian, M., Li, L.,
539 Liang D., Li, C., 2009. Influence of anchoring ligands and particle size on the colloidal
540 stability and in vivo biodistribution of polyethylene glycol-coated gold nanoparticles
541 in tumor-xenografted mice. Biomaterials 30, 1928–1936.
542 https://doi.org/10.1016/j.biomaterials.2008.12.038
543 Zhang, S., Moustafa, Y., Huo, Q., 2014. Different Interaction Modes of Biomolecules with
544 Citrate-Capped Gold Nanoparticles. ACS Appl. Mater. Interfaces 6, 21184–21192.
545 https://doi.org/10.1021/am506112u
546 Zopes, D., Stein, B., Mathur, S., Graf, C., 2013. Improved Stability of “Naked” Gold
547 Nanoparticles Enabled by in Situ Coating with Mono and Multivalent Thiol PEG
548 Ligands. Langmuir 29, 11217–11226. https://doi.org/10.1021/la4012058
549

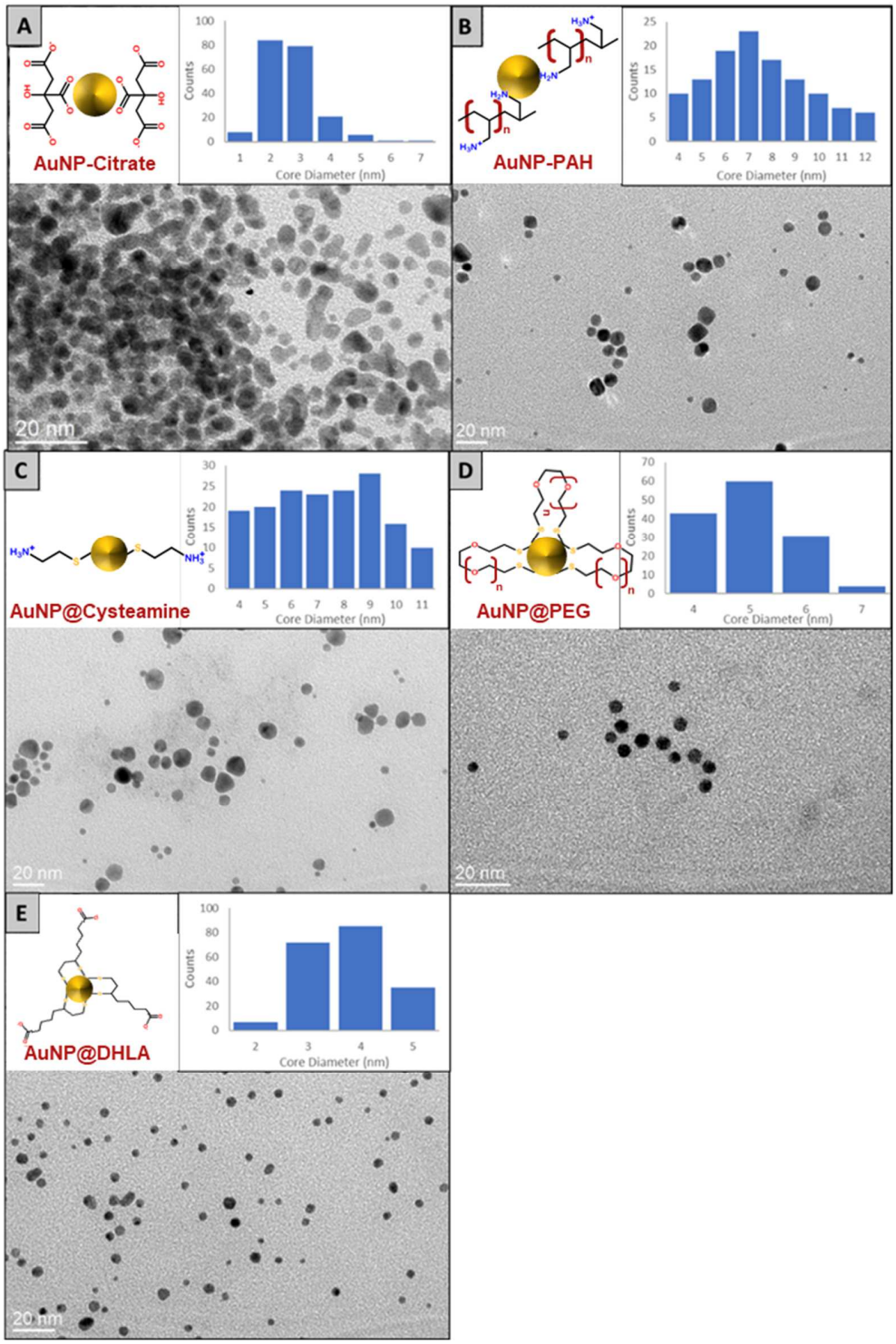


Figure 1. Observation by TEM of AuNP stabilized by citrate (A), PAH (B), capped by cysteamine (C), DHLA (D) and PEG (E) and histograms representing AuNP Dc measured on at least 150 individualized particles. Schematic representations of the studied nanoparticles are also represented.

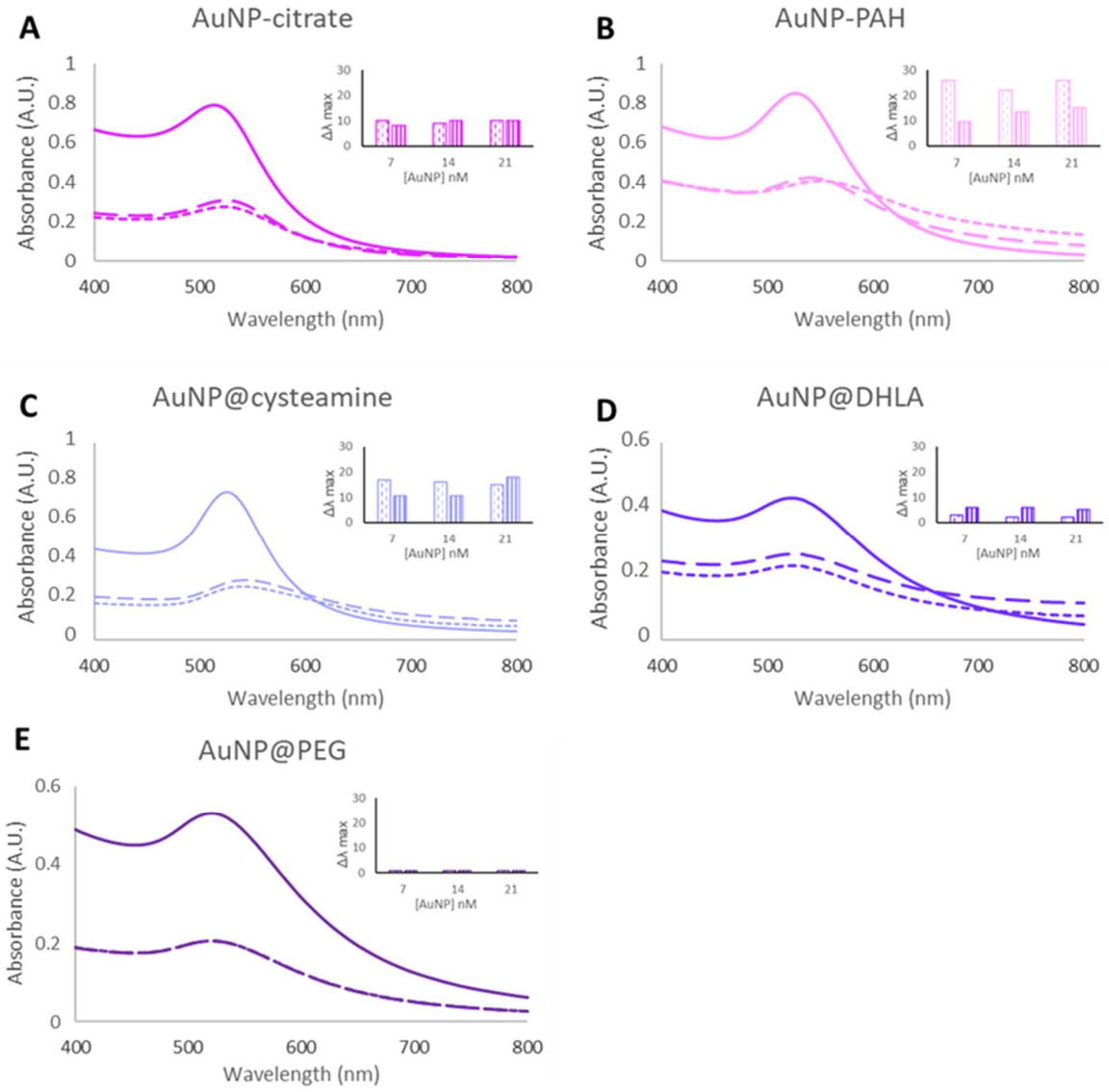


Figure 2. Typical visible spectra of citrate, PAH, cysteamine AuNP(A,B,C) at 70 nM and DHLA, PEG AuNP at 50 nM (solid line) and spectra of AuNP (21 nM) mixed with either albumin (short dashed lines) or fibrinogen (long dashed lines) at 50 nM. Histograms represent the variation of the Surface Plasmon Band wavelength after mixing AuNP (at 7, 14, and 21 nM) with albumin (short dashed) or fibrinogen (long dashed) at 50 nM.

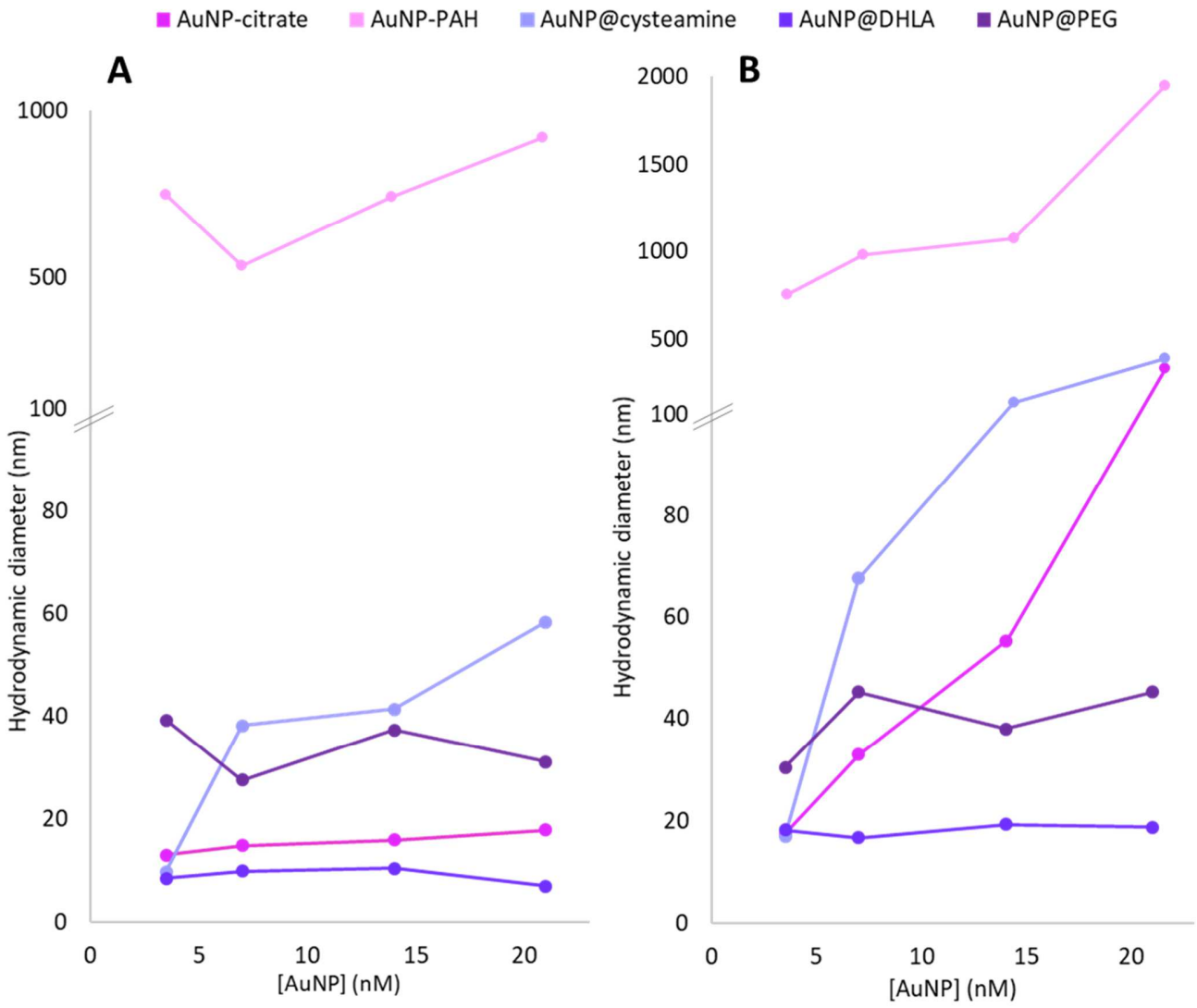


Figure 3. AuNP Dh measured by Dynamic Light Scattering. AuNP concentrations were increased from 3.5 nM to 21 nM in interaction with either albumin (A) or fibrinogen (B) which concentrations were fixed at 50 nM.

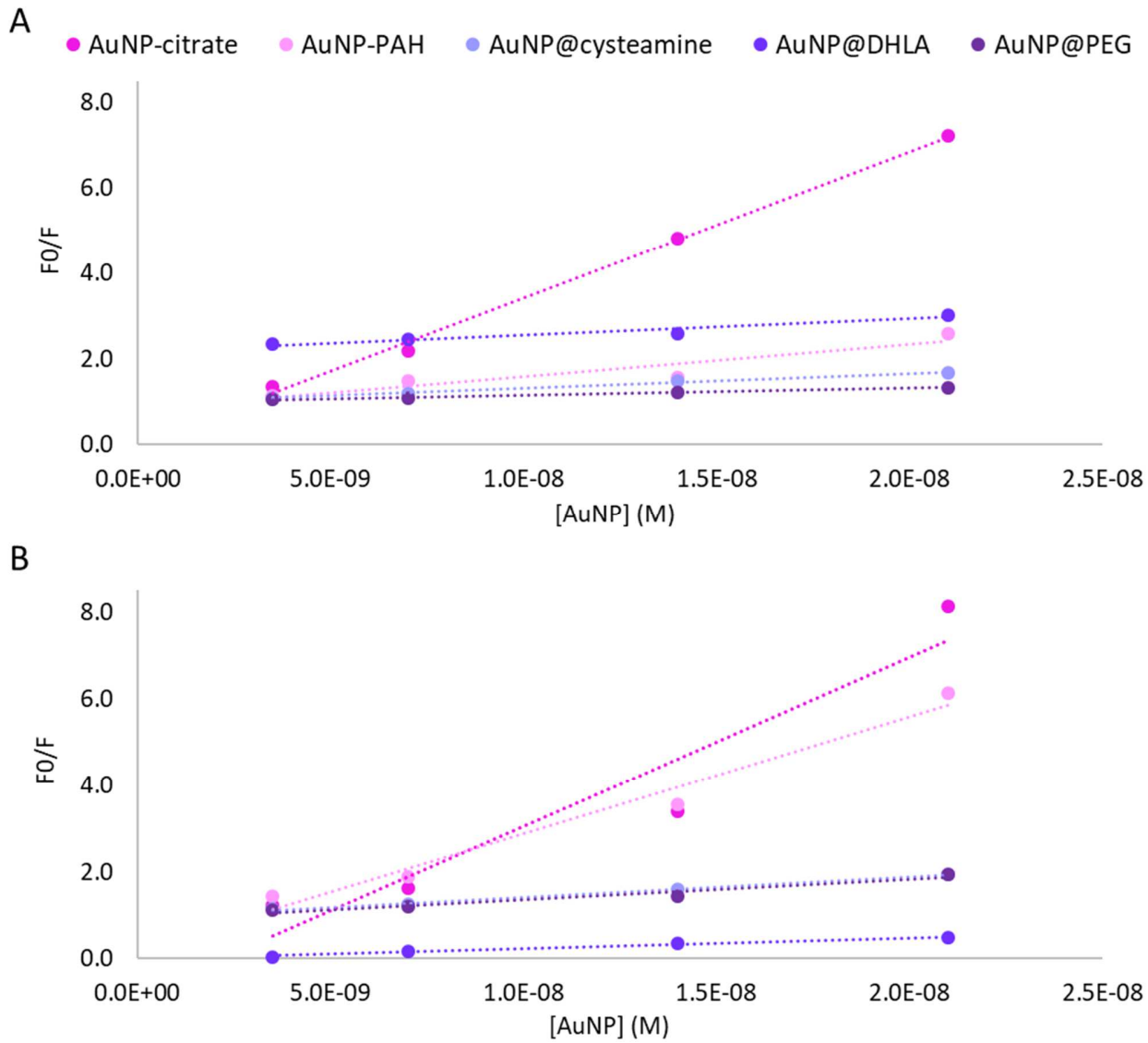


Figure 4. Stern-Volmer plot at 37 °C determined through fluorescence quenching of albumin (A) and fibrinogen (B) by an increasing concentration of AuNP.

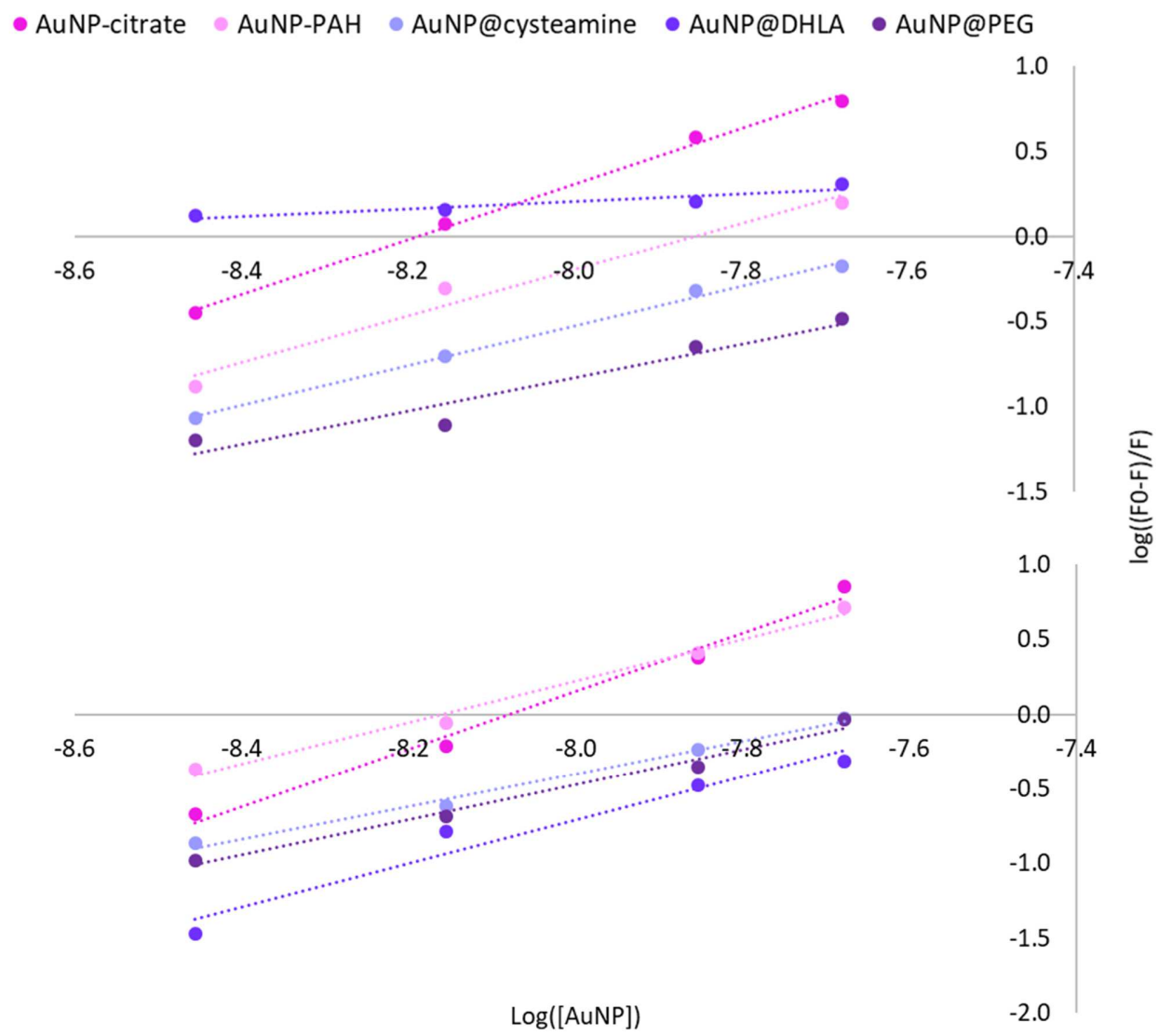


Figure 5. Ka plot at 37 °C determined through fluorescence quenching of albumin (A) and fibrinogen (B) by an increasing concentration of AuNP.

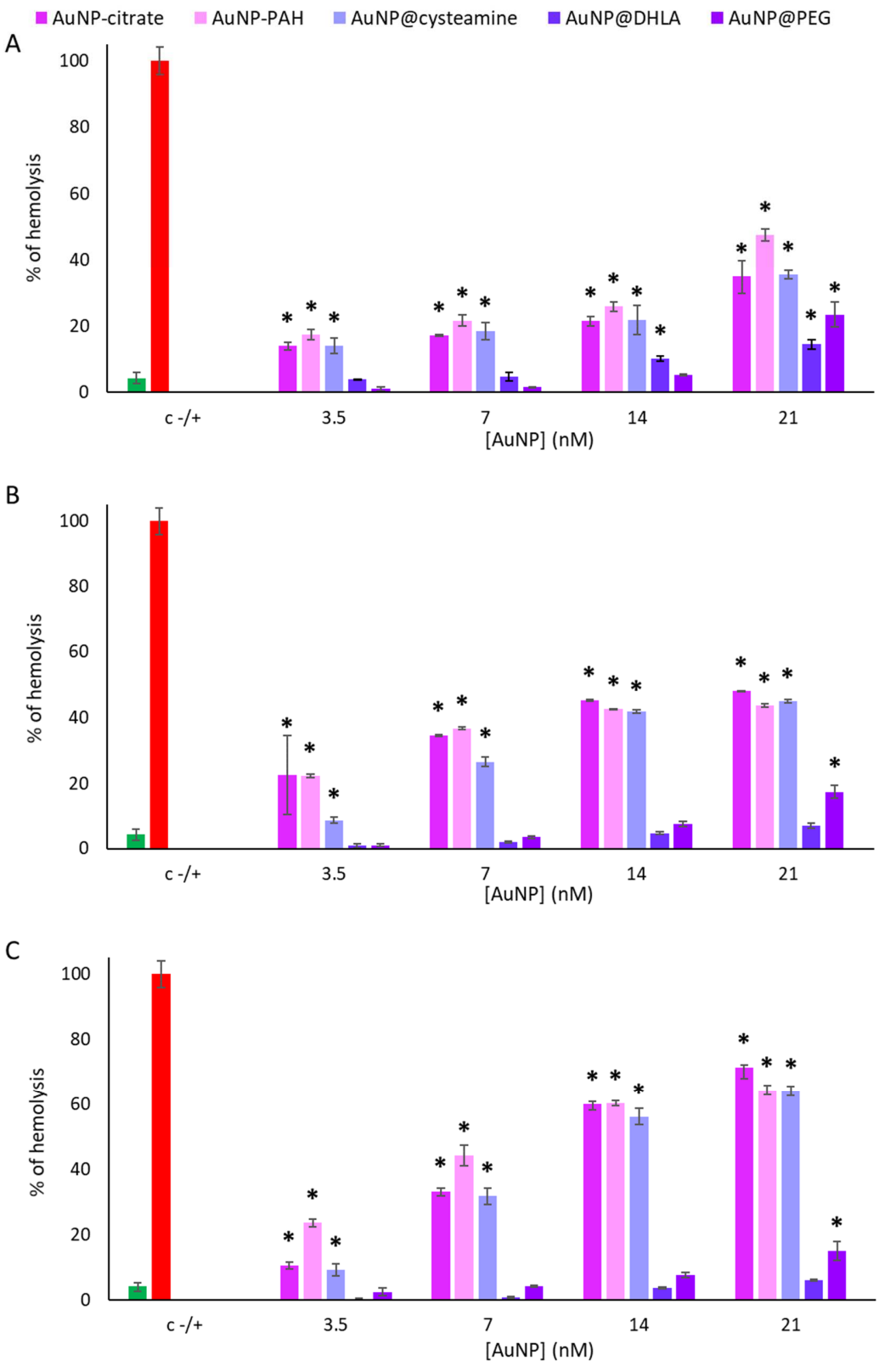

AuNP-citrate
AuNP-PAH
AuNP@cysteamine
AuNP@DHLA
AuNP@PEG
A
B
C
% of hemolysis
0
20
40
60
80
100
c -/+
3.5
7
14
21
[AuNP] (nM)

Figure 6. Hemolysis ratio (n = 3), errors bars represent the standard deviation) induced by an increasing concentration of AuNP in PBS (except for negative and positive controls) without proteins (A), or with either albumin at 50 nM (B) or fibrinogen at 50 nM (C). Statistical analyses were performed through two-way ANOVA followed by a post-hoc Bonferroni test (* $p < 0.001$ vs negative control)

Table 1. Physicochemical parameters of human proteins used in this study.

Physicochemical properties	Albumin	Fibrinogen
Molecular mass ($g.mol^{-1}$)	69 000	340 000
Isoelectric point	4.7	5.8
Net charge at pH = 7.4 (mV)	-26	-38
Number of tryptophan residues accessible for quenching	1	25 [a]
Dimensions (nm)	7 × 6 × 4 [b]	9 × 47 × 6 [c]
Shape	Heart	Rodlike

a:(Gonçalves et al., 2007) b:(Erickson, 2009) c: (Cieśla et al., 2013)

Table 2: Physicochemical characterization of colloidal gold nanoparticles (n = 3 on three independent syntheses).

Physicochemical parameter	AuNP-Citrate	AuNP-PAH	AuNP@ Cysteamine	AuNP@ DHLA	AuNP@ PEG
λ max (nm)	514 ± 1	528 ± 2	522 ± 3	521 ± 2	518 ± 1
Hydrodynamic diameter Dh (nm)	5.8 ± 0.9	11.9 ± 0.7	10.5 ± 1.5	8.4 ± 0.9	28.5 ± 0.5
Core diameter Dc (nm)	2.7 ± 0.8	7.4 ± 2.1	7.3 ± 2.0	5.0 ± 0.7	3.7 ± 0.8
Zeta potential ζ (mV)	-32 ± 1	31 ± 3	28 ± 2	-46 ± 3	-4 ± 2
Ligand binding Energy ($kJ.mol^{-1}$)	11[a]	25[b]	188[c]	188[c]	188[c]

a: energy per interaction Au-O involved in the stabilization of the gold core by citrate ions (Al-Johani et al., 2017), b: energy per interaction Au-N (Nuzzo et al., 1987) involved in the stabilization of the gold core by poly(allylamine), c: binding energy of a single thiol on AuNP gold core (Nuzzo et al., 1987), note that in the case of DHLA and PEG capping two thiols each ligand molecule is bound by two thiols.

Table 3. AuNP Dh and external layer thickness at a concentration of 7 nM.

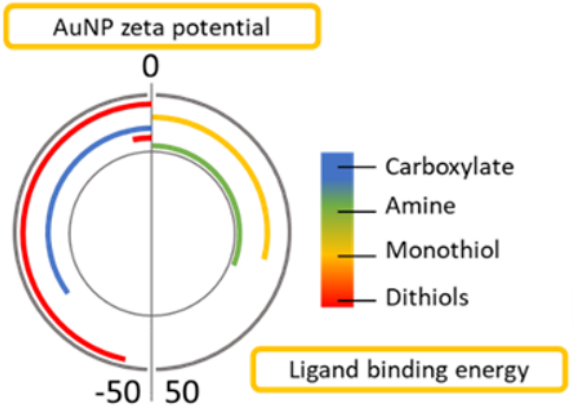
	Dh (nm)			External layer thickness (nm)	
AuNP concentration	7 nM				
Protein	none	Albumin	Fibrinogen	Albumin	Fibrinogen
AuNP-citrate	5.8	14.8	32.9	12.1	Aggregation above 3.5 nM
AuNP-PAH	11.9	537	981	Aggregation	
AuNP@Cysteamine	4.4	38.2	67.7	Aggregation above 3.5 nM	
AuNP@DHLA	8.4	9.9	16.7	4.9	11.7
AuNP@PEG	28.3	27.5	45.3	23.8	41.6

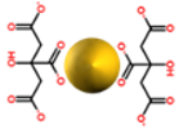
Table 4. Albumin and fibrinogen fluorescence quenching constants at 37 °C. R stands for the correlation coefficient.

		AuNP ligand				
	Protein	Citrate	PAH	Cysteamine	DHLA	PEG
K_{sv} (L.mol^{-1})	Albumin	3.4×10^{8}	7.5×10^{7}	3.4×10^{7}	3.8×10^{7}	1.6×10^{7}
	Fibrinogen	3.9×10^{8}	2.7×10^{8}	4.7×10^{7}	2.6×10^{7}	5.0×10^{7}
K_q (L.mol^{-1}. s^{-1})	Albumin	3.4×10^{15}	7.5×10^{14}	3.4×10^{14}	3.8×10^{14}	1.6×10^{14}
	Fibrinogen	3.9×10^{15}	2.7×10^{15}	4.7×10^{14}	2.6×10^{14}	5.0×10^{14}
R	Albumin	0.9984	0.9343	0.9964	0.9708	0.9896
	Fibrinogen	0.9553	0.9861	0.9974	0.9932	0.9869

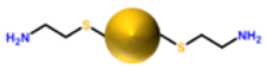
Table 5. Thermodynamics constants of AuNP- albumin or fibrinogen complexation at 37°C

		AuNP ligand				
	Protein	Citrate	PAH	cysteamine	DHLA	PEG
Hill coefficient	Albumin	1.6	1.2	1.2	0.2	1.0
	Fibrinogen	2.3	1.5	1.3	1.0	1.2
Ka	Albumin	1.8×10^{13}	4.8×10^{10}	6.3×10^{8}	8.1×10^{1}	3.1×10^{7}
	Fibrinogen	1.7×10^{18}	3.6×10^{12}	8.1×10^{9}	6.1×10^{7}	2.5×10^{9}
ΔS ($J.K^{-1}.mol^{-1}$)	Albumin	-432	-227	-501	-88	821
	Fibrinogen	574	-278	189	225	123
ΔH ($kJ.mol^{-1}$)	Albumin	-200	-106	-208	-37	207
	Fibrinogen	69	-157	104	-45	-18
ΔG ($kJ.mol^{-1}$)	Albumin	-65	-35	-53	-9	-48
	Fibrinogen	-54	-52	-48	-50	-56
Interaction	Albumin	H bound and Van Der Waals bound				Hydrophobic/ ionic
	Fibrinogen	Hydrophobic/ ionic	H bound and Van Der Waals bound	Hydrophobic/ ionic	Ionic	Ionic





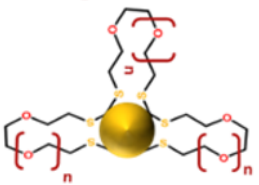
AuNP-Citrate



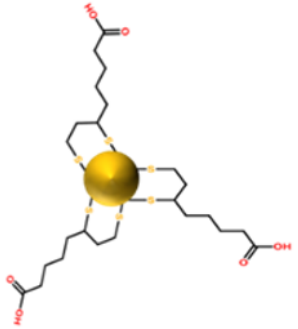
AuNP@Cysteamine



AuNP-PAH



AuNP@PEG



AuNP@DHLA